https://arabjchem.org

Arabian Journal of Chemistry

2025 18 (2) 92024

Original Article

Analysis of the mechanism of *Eleutherococcus senticosus* inducing ferroptosis in the treatment of gastric cancer by integrating network pharmacology, transcriptome, and metabolomics

Xin Song[†,a], Yufeng Li[†,b], Dan Li[b], Zhuo Wang[b], Xuekun Kou[a], Xiaohui Zhang[b], Yuanyuan Zhao[b], Chunqiu Liu[b], Yuehong Long[a,*], Jingwu Li[b,*], Zhaobin Xing[a,*]

[a]*College of Life Sciences, North China University of Science and Technology, Tangshan-063210, China*
[b]*Hebei Key Laboratory of Molecular Oncology, Tangshan People's Hospital, Tangshan-063000, China*

ARTICLE INFO

Keywords:
Eleutherococcus senticosus
Ferroptosis
Gastric cancer
Metabolome
Molecular dynamics simulation
Transcriptome

ABSTRACT

Various components of the traditional medicine *Eleutherococcus senticosus* (*E. senticosus*) exhibit anti-cancer effects, but the specific components and mechanisms of ferroptosis in gastric cancer (GC) have not been clarified. This study aims to identify how *E. senticosus* induces ferroptosis in GC through network pharmacology, experimental validation, and integrated transcriptomics and metabolomics analysis, using molecular docking and kinetic simulations to predict the core active components of *E. senticosus*. Multiple active ingredients of *E. senticosus* were found to influence ferroptosis in GC cells via various pathways. First, *E. senticosus* significantly decreased glutathione levels and increased malondialdehyde and unsaturated fatty acid synthesis precursors in GC cells. Transcriptomic and metabolomic analyses revealed significant alterations in genes and metabolites related to the ferroptosis pathway in GC cells. *EGFR* (epidermal growth factor receptor), *TFRC* (transferrin receptor), *ACSL4* (long-chain acyl-CoA synthetase 4), *GPX4* (glutathione peroxidase 4), and *FTH1* (ferritin heavy chain 1) were identified as core target genes showing the highest correlation. Next, the results of cellular validation experiments showed that the treatment of *E. senticosus* significantly upregulated the genes that promote ferroptosis and downregulated inhibitory genes. Molecular docking and dynamics simulations identified syringin, ciwujianoside I, ursolic acid, ciwujianoside B, and quercetin as active components of *E. senticosus* acting on these core targets. In summary, *E. senticosus* may act on *EGFR*, *TFRC*, *ACSL4*, *GPX4*, and *FTH1* through syringin, ciwujianoside I, ursolic acid, ciwujianoside B, and quercetin, respectively, modulating their expression to disrupt GC cell homeostasis and promote ferroptosis.

1. Introduction

Gastric cancer (GC) is among the most prevalent malignant tumors, showing increasing incidence in recent years, which ranks fifth in incidence and fourth in mortality among various malignancies, significantly impacting patient health [1]. Surgical resection remains the primary treatment for GC; however, many patients with advanced stage GC miss this opportunity, resulting in poor prognosis. The median survival with chemotherapy-based treatment is generally less than one year [2]. The short-term prognosis of patients with GC has been improved with the application of adjuvant chemotherapy and the development of new targeted drugs. However, drug resistance often emerges, leading to unsatisfactory long-term prognosis for patients with GC [3]. Thus, a deep understanding of the biological mechanism of GC is crucial for developing new drugs and therapeutic targets. Resistance to cell death is an important feature of cancer, and GC cells are also resistant to treatment in this way, necessitating novel strategies to induce GC cell death.

Ferroptosis is a new type of cell death [4]. Abnormal iron and lipid metabolism and the production of reactive oxygen species (ROS) distinguish cancer cells from normal cells [5]. This vulnerability to ferroptosis suggests that it is a novel method to combat drug-resistant cancers [6]. It has been shown that body iron stores, as measured by serum iron and ferritin, are negatively correlated with GC risk [7]. Conversely, iron deficiency increases oxidative stress and deoxyribonucleic acid (DNA) damage and increases the risk of cancer, particularly evident in the development of gastrointestinal tumors. The combination of ferroptosis activators and antitumor drugs or induction of ferroptosis in tumor cells is beneficial to the intervention, inhibition, and clearance of GC [8]. This suggests that although the role of iron in GC development remains to be further investigated, the fact that it can influence tumorigenesis and progression through the ferroptosis pathway has been confirmed by numerous experiments [9].

Modern studies have revealed the presence of antitumor-active ingredients in Chinese herbal medicine extracts, including polysaccharides, saponins, and steroids [10]. *Eleutherococcus senticosus* (*E. senticosus*), a traditional Chinese medicinal plant, also known as Siberian ginseng, has high medicinal value and is often classified as an "adaptogen" alongside *Panax ginseng* [11]. *E. senticosus*

***Corresponding authors:**
E-mail addresses: longyh@ncst.edu.cn (Y. Long), tslijingwu@163.com (J. Li), xingzb@ncst.edu.cn (Z. Xing)
[†]Authors contributed equally to this work and shared co-first authorship.

Received: 08 September, 2024 **Accepted:** 08 December, 2024 **Epub Ahead of Print:** 10 March 2025 **Published:** 18 March 2025
DOI: 10.25259/AJC_9_2024

exhibits antibacterial, anti-cancer, anti-fatigue, anti-inflammatory, anti-stress, and immunostimulatory effects [12]. Syringin and *E. senticosus* polysaccharides are identified as key active components of the antitumor effect of *E. senticosus* [13]. Syringin can inhibit the proliferation of breast, lung, prostate, and pancreatic cancers [14]. *E. senticosus* polysaccharides have an inhibitory effect on the proliferation of human lung cancer H446 cells, which can block the cell cycle by increasing the activation of extracellular regulated kinase (*ERK*) and *P38* [11].

While *E. senticosus* polysaccharides enhance immune system resistance and alter biochemical characteristics of membrane phospholipids to exert their antitumor effects, their specific pathways affecting GC ferroptosis and the mechanism of action of active ingredients remain unclear. Hence, this study uses multiomics and multilevel approaches to preliminarily analyze the mechanism of *E. senticosus* in GC treatment through ferroptosis.

2. Materials and Methods

2.1. Screening of active compounds of E. senticosus and acquisition of targets

The active compounds of *E senticosus* and their targets, GC-related gene targets, and ferroptosis-related gene targets were screened by reference methods [15]. The main targets were obtained by removing duplicate values and Uniport (https://www.uniprot.org/) database standardization.

2.2. Construction of protein-protein interaction network

The intersection of the corresponding targets, GC targets, and ferroptosis targets of *E. senticosus* was obtained using the Metware Cloud platform (https://cloud.metware.cn). STRING (https://string-db.org/) was used to construct a protein-protein interaction (PPI) network. The core targets of *E. senticosus* affecting GC ferroptosis were determined using multiple algorithms [15].

2.3. Functional enrichment analysis

Metascape (https://www.metascape.org/gp/index.html) was used to analyze the signal pathways and gene functions of the intersection targets. Function enrichment analysis of genes were performed using the method of reference, and visual processing was performed [15].

2.4. Bioinformatics analysis and molecular docking

The messenger ribonucleic acid (mRNA) expression level of the core target and its relationship with the survival curve were analyzed by reference method [15]. Molecular docking and dynamic simulation analysis were carried out according to the method of literature [16]. The structural protein conformation of the main active compounds was derived from the a protein data bank (https://www.rcsb.org/) database. AUTODOCK VINA was used to evaluate the molecular interaction between the core protein and the corresponding ligand, and the binding pocket was identified autonomously.

2.5. Identification of AGS cells and treatment of AGS cells by E. senticosus

AGS cells were obtained from the Zhongke Dixian Science and Technology Development Company Limited (China). AGS cells in the control group were cultured in the reference method [15]. The experimental groups were treated with final concentrations of 15, 20, 25, 30, and 35 mg/mL of *E. senticosus* powder (Henan Longteng Bioengineering Company, China) in the same complete medium and cultured at 37°C in a 5% carbon dioxide (CO_2) incubator for 48 hrs. Four biological replicates were set for all experiments.

2.6. Metabolomic and transcriptome analysis of AGS cells treated with E. senticosus

Metabolomic analysis of AGS cells treated with *E. senticosus* was performed by the reference method [17]. Total ribonucleic acid (RNA) was extracted from AGS cells in the 25 mg/mL *E. senticosus* treatment group and from the control group using the Trizol method and reverse transcribed into complementary DNA (cDNA). The sequencing data was spliced and assembled, and UniGene annotation information was obtained by comparison with multiple databases such as kyoto encyclopedia of genes and genomes (KEGG) and non-redundant protein database (NR) [12]. The expression and differentially expressed metabolites and genes were screened by the reference method [18].

2.7. Determination of cell viability

Cell viability was detected using a Multiskan FC microplate reader (Thermo Fisher, USA) to measure the absorbance of AGS cells treated with cell counting kit-8 solution in the control group and *E. senticosus*. The IC50 value was calculated by the reference method [11]. Assay kits (Abcam, UK) were used to evaluate the contents of malondialdehyde (MDA) and glutathione (GSH) in cell lysates.

2.8. Quantitative real time and western blot

Reference method, using StepOne real-time polymerase chain reaction (PCR) system (Applied Biosystems, China) for real-time quantitative reverse transcription polymerase chain reaction (qRT-PCR). Glyceraldehyde-3-phosphate dehydrogenase (*GAPDH*) was used as an internal reference gene. Primer sequences are shown in Table S1. Western Blot experiment was carried out according to the literature method [13]. The antibodies were all derived from PTM BioLab, China, using Image Quant LAS-4000 (Genetal Electric, Boston, USA) for membrane visualization.

2.9. Statistical analysis

Data were analyzed by SPSS (version 18.0) and comparison between groups was analyzed by one-way ANOVA [14]. The experimental results were expressed as the mean ± SD. $P < 0.05$ was considered statistically significant.

3. Results and Discussion

3.1. Screening of active compounds and potential targets of E. senticosus

A total of 72 active components were initially found in *E senticosus*. After summarizing and eliminating duplicate data, 46 components were found to have corresponding target genes (Table S2). Predicting and removing duplicate values from the database yielded a total of 523 potential targets for these ingredients. Screening identified 12,823 GC- and 467 ferroptosis-related targets. Combining these three sets yielded a total of 61 common targets (Figure 1a, Table S3). The active compounds associated with these 61 common targets include syringin, ciwujianoside I, ursolic acid, ciwujianoside B, quercetin, 4-coumaric acid, oleanolic acid, and isofraxidin, which are potential inducers of GC ferroptosis by *E. senticosus*.

The protein-protein interaction (PPI) network analysis of 61 common targets showed that there were 61 nodes and 546 edges, and the average node value of common targets was 17.6 (Figure 1b). The molecular complex detection (MCODE) plug-in identified one protein module with an evaluation score of 23.2, involving 26 key targets, forming the MCODE set (Table S4).

Gene ontology (GO) analysis revealed that common targets are involved in 942 biological processes (BPs), 33 cellular components (CCs), and 90 molecular functions (MFs) (Figure 1c). BP enrichment analysis indicated that many target genes participate in processes such as cell response to ROS and metal ions. CC enrichment analysis highlighted associations with membrane microdomains and transcription regulator complexes. MF enrichment analysis showed involvement in iron ion binding, fatty acid binding, nuclear receptor activity, mitogen-activated protein kinase (MAPK) activity, and oxidoreductase activity.

Kyoto Encyclopedia of Genes and Genomes (KEGG) analysis identified a total of 159 pathways (Figure 1d), with the top ten pathways in cancer being lipid and atherosclerosis, hypoxia-inducible factor-1 (HIF-1) signaling pathway, efferocytosis, necroptosis, Janus kinase-

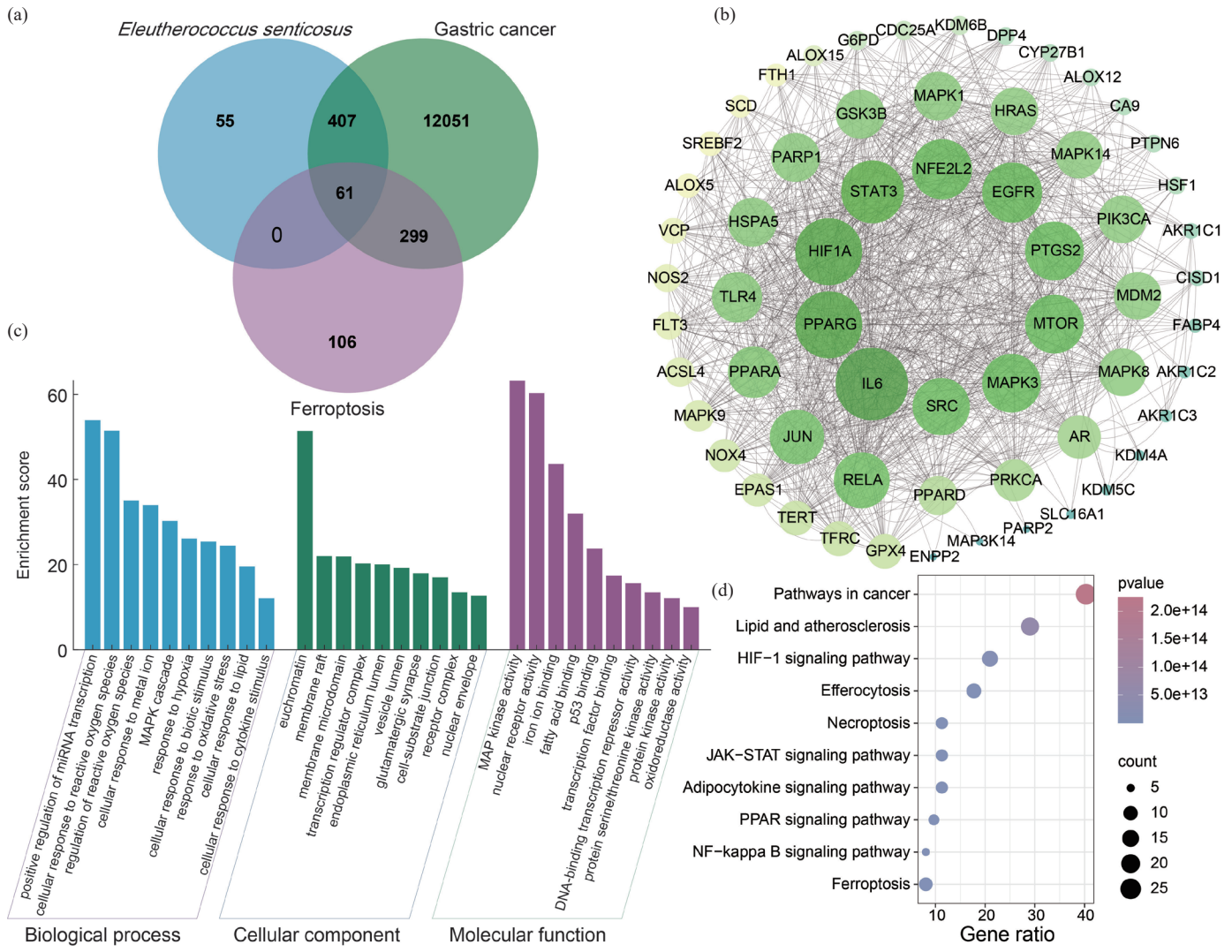

Figure 1. Analysis of corresponding targets, disease targets, and ferroptosis targets of *E. senticosus*. (a) The intersection of corresponding targets, disease targets, and ferroptosis targets of *E. senticosus.* (b) Protein-protein interaction (PPI) network of intersection targets. (c) Gene ontology (GO) analysis of intersection targets. (d) Kyoto encyclopedia of genes and genomes (KEGG) pathway enrichment analysis of intersection targets.

signal transducer and activator of transcription (JAK-STAT) signaling pathway, adipocytokine signaling pathway, peroxisome proliferator-activated receptor (PPAR) signaling pathway, nuclear factor kappa-light-chain-enhancer of activated B cells (NF-κB) signaling pathway, and ferroptosis. These findings suggest that *E. senticosus* may induce ferroptosis in GC cells through these pathways.

3.2. Bioinformatics analysis

Using the GEPIA database revealed (Figure S1) the mRNA expression levels of Long-chain acyl-CoA synthetase 4 (*ACSL4),* Glutathione peroxidase 4 *(GPX4), HIF-1A, PARP1* (polymerase 1), and transferrin receptor (*TFRC)* were significantly increased (Figure 2a) ($P < 0.05$). The mRNA expression levels of other genes were not significantly different.

Survival curve analysis of key targets (Figure S2) indicated that *AR* (androgen receptor), *GPX4*, and *PTGS2* (prostaglandin-endoperoxide synthase 2) genes were significantly associated with prognostic values (Figure 2b; $P < 0.05$).

3.3. Cell experiment and ferroptosis index detection

The cell viability assay results demonstrated a gradual increase in the inhibition rate of AGS cells treated with *E. senticosus* as the concentration increased (Figure 3a). The IC50 of *E. senticosus* on AGS cells was approximately 25.16 mg/mL. Additionally, the colony formation assay indicated a significant inhibition of AGS cell colony formation with prolonged treatment time or higher concentrations of *E. senticosus* compared to the control group (Figure 3b).

Furthermore, *E. senticosus* treatment led to a significant reduction in the levels of GSH in AGS cells (Figure 3c). As the concentration of *E. senticosus* increased, there was a marked decrease in GSH content in AGS cells ($P < 0.001$). The levels of the ferroptosis marker MDA in AGS cells following treatment with *E. senticosus* are shown in Figure 3(d). The accumulation of malondialdehyde (MDA) increased significantly with increasing concentrations of *E. senticosus* ($P < 0.05$ or $P < 0.01$), suggesting that *E. senticosus* may promote the occurrence of ferroptosis in AGS cells.

3.4. Effect of E. senticosus treatment on metabolic characteristics of AGS cells

The results of principal component analysis in positive and negative ion modes (Figure 4a) revealed that samples within the same treatment group clustered closely together. At the same time, distinct clustering was observed between groups. The metabolic profiles were further validated using partial least squares discriminant analysis (PLS-DA) (Figure 4b), demonstrating significant separation between the two groups, indicative of substantial metabolic changes in AGS cells following *E. senticosus* treatment. In the negative ion mode, $R^2Y = 0.9921$ and $Q^2 = 0.051$, and in the positive ion mode, $R^2Y = 0.9845$ and $Q^2 =$

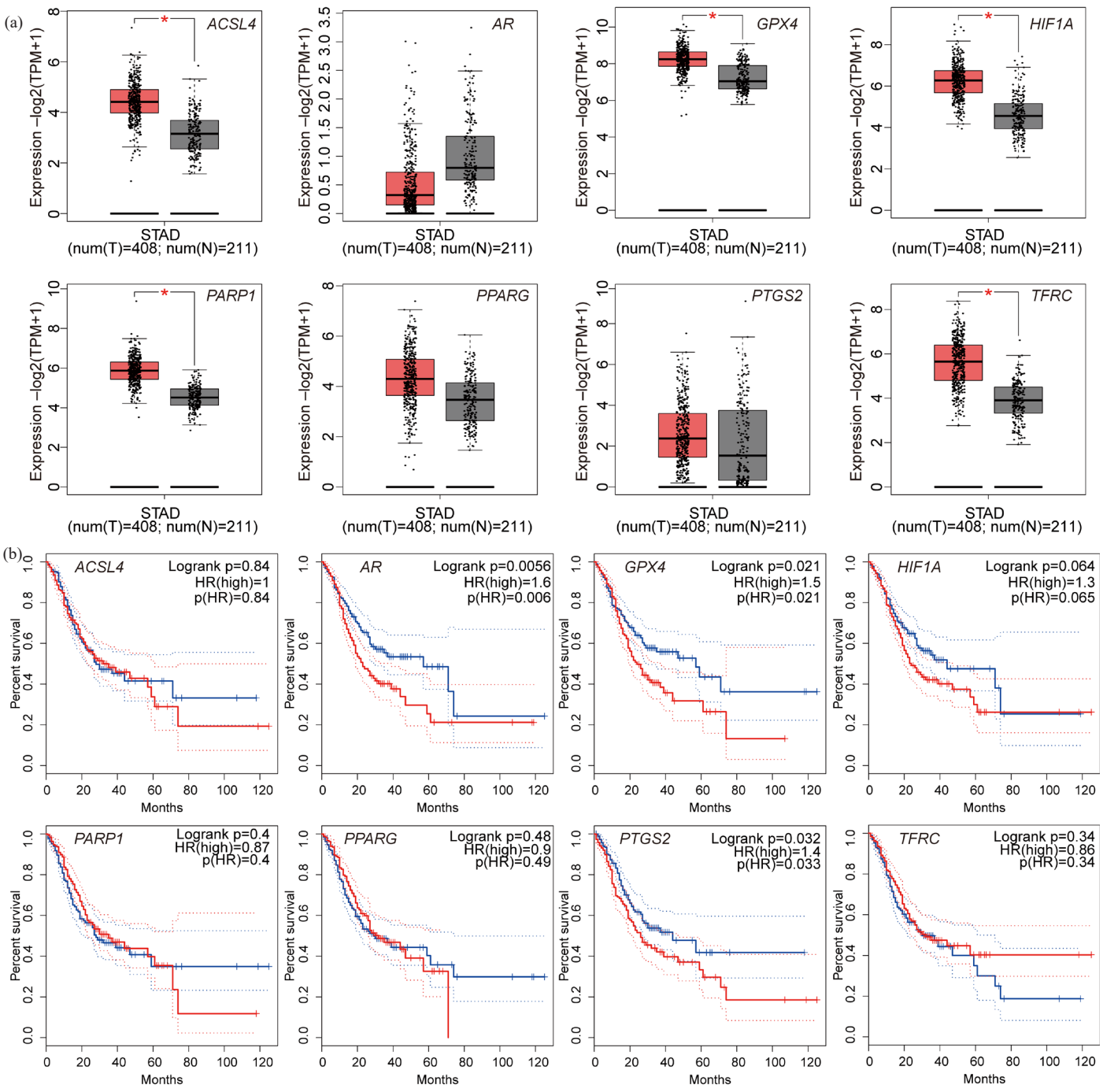

Figure 2. mRNA expression level and survival analysis curve of core targets. (a) mRNA expression level of core targets: red represents gastric cancer and gray represents normal tissue. (b) Survival analysis curve of gastric cancer patients with high (red) and low (blue) expression targets (*$P < 0.05$). (ACSL4: Long-chain acyl-coa synthetase 4, AR: Androgen receptor, GPX4: Glutathione peroxidase 4, HIF1A: Hypoxia inducible factor 1 alpha, PARP1: Poly adp-ribose polymerase-1, PPARG: Peroxisome Proliferator Activated Receptor Gamma, PTGS2: Prostaglandin-endoperoxide synthase 2, TFRC: Transferrin receptor, HR: HR Lysine Demethylase and Nuclear Receptor Corepressor, STAD: Stomach adenocarcinoma).

0.6939. Lower Q^2 and R^2Y values on the left and green sides indicate a low risk of overfitting in PLS-DA for both ion modes, confirming robust reproducibility of the metabolomic analysis (Figure 4c).

A total of 932 metabolites were detected in AGS cells treated with *E. senticosus*, of which 144 were differential metabolites, belonging to ten categories (Figure 4d, Table S5, Figure S3). KEGG enrichment analysis showed these metabolites were enriched in 94 signaling pathways (Table S6, Figure S4). The top 20 signaling pathways, prominently featuring ferroptosis, included ten enriched metabolites crucial to this pathway: 3-hydroxy-3-methylglutaryl coenzyme A (HMG-CoA), acetyl-CoA, pulmonary embolism-Arachidonic acid (PE-AA), lyso-PE, Oxidized glutathione (GSSG [glutathione disulfide]), reduced GSH, γ-glutamylcysteine (γ-GC), Cys, and Glutamate (Glu.)

GSH, a critical regulator of intracellular ferroptosis, and its associated metabolites are pivotal in mitigating this process. *E. senticosus* treatment significantly reduced levels of GSH, Glu, and Cys by 80.42%, 71.63%, and 63.95%, respectively, suggesting inhibition or disruption of GSH metabolism (Figure 4e). Additionally, the synthesis of unsaturated fatty acids, another crucial substrate in ferroptosis, was notably affected by *E. senticosus*, with linoleic acid increasing by approximately 52.62% posttreatment. Furthermore, lipid peroxide synthesis intermediates such as lysoPE, acetyl-CoA,

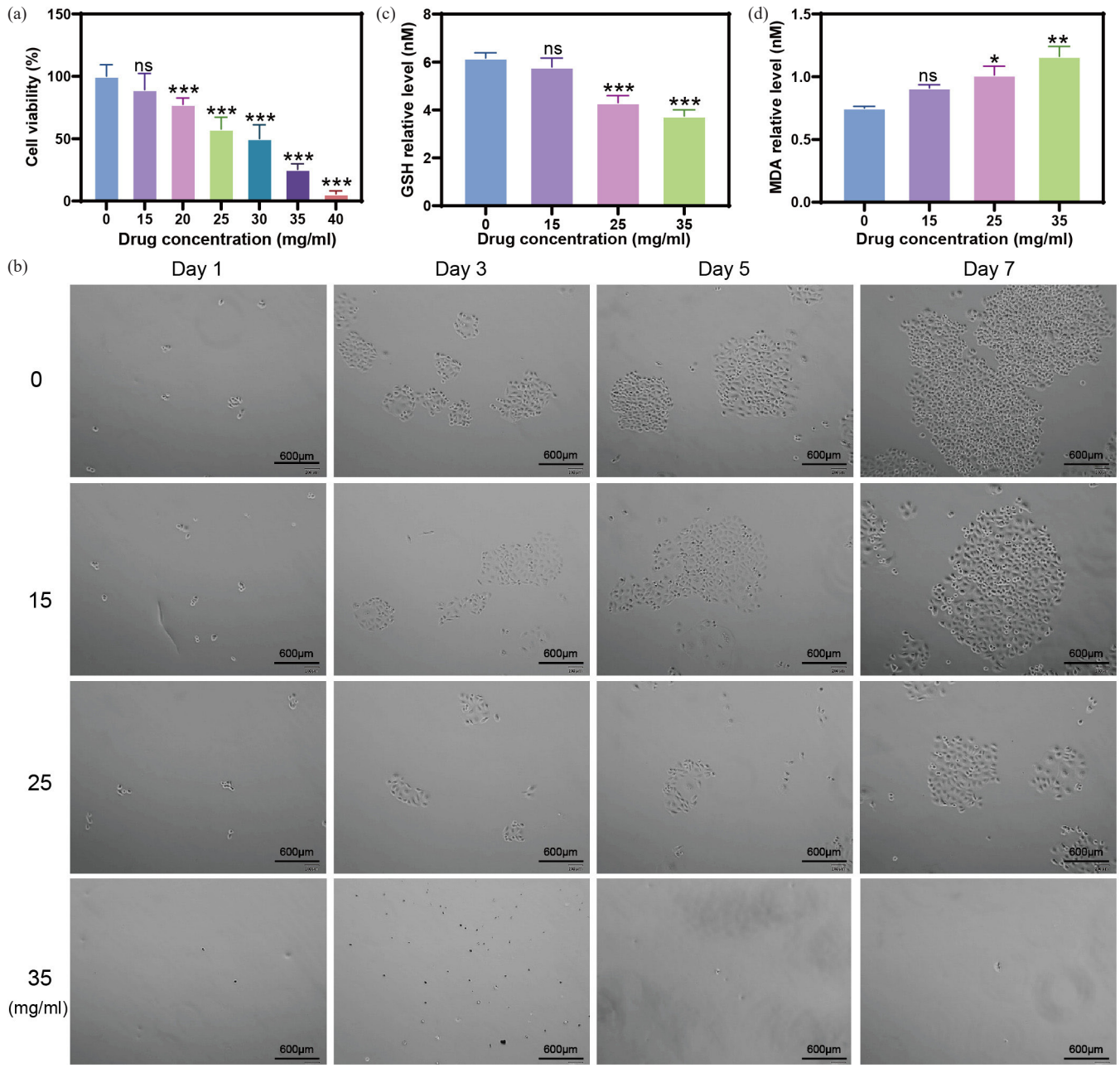

Figure 3. Effects of *E. senticosus* on proliferation and growth of AGS cells. (a) Inhibition rate of AGS cells by *E. senticosus*. (b) Effect of *E. senticosus* on the growth of AGS cells. (c and d) Effect of *E. senticosus* on the content of glutathione and malondialdehyde in AGS cells (* $P < 0.05$, ** $P < 0.01$, and *** $P < 0.001$). (Blue represents the concentration of *E. senticosus* at 0 mg/ml, light purple represents the concentration of *E. senticosus* at 15 mg/ml, pink represents the concentration of *E. senticosus* at 20 mg/ml, light green represents the concentration of *E. senticosus* at 25 mg/ml, dark green represents the concentration of *E. senticosus* at 30 mg/ml, deep purple represents the concentration of *E. senticosus* at 35 mg/ml, and orange represents the concentration of *E. senticosus* at 40 mg/ml correspond to the concentration of *E. senticosus* in the abscissa axis.)

and PE-AA was significantly elevated in the *E. senticosus*-treated group (Figure 4f).

3.5. Effect of E. senticosus treatment on gene transcription of AGS cells

RNA-seq (RNA sequencing) analysis revealed significant transcriptional alterations induced by *E. senticosus* treatment in AGS cells, affecting 229 genes (Figure S5 and S6). Of these, 126 genes were upregulated, while 103 were downregulated (Figure 5a,b). The KEGG pathway enrichment results of these differentially expressed genes showed that there were mainly ferroptosis, metabolic pathways, steroid hormone biosynthesis, and chemical carcinogenesis-receptor activation (Figure 5c). Among the differentially expressed genes, eight ferroptosis-related genes exhibited upregulation while six were downregulated. *GPX4* and Ferritin heavy chain 1 (*FTH1)* gene expressions decreased by 40.26% and 37.63%, respectively. In contrast, Epidermal growth factor receptor (*EGFR)*, *TFRC*, and *ACSL4* expressions increased by 77.59%, 91.46%, and 78.22%, respectively (Figure 5d). Additionally, nine genes related to metabolic pathways showed upregulation while six were downregulated. Genes involved in steroid hormone biosynthesis were upregulated by three and downregulated by five. In contrast, chemical carcinogenicity-receptor activation-related genes exhibited upregulation and downregulation in three cases (Figure 5c).

3.6. Screening and verification of core targets

We analyzed the correlation between ferroptosis-related genes and metabolites to identify the core targets of *E. senticosus*-induced ferroptosis in AGS cells. The results revealed varying degrees of correlation between the expression of nine genes and 14 metabolites (Figure 6a). *ACSL4* showed the strongest correlation with unsaturated fatty acid ALA, with a correlation coefficient (R) of 0.881231. *TFRC*

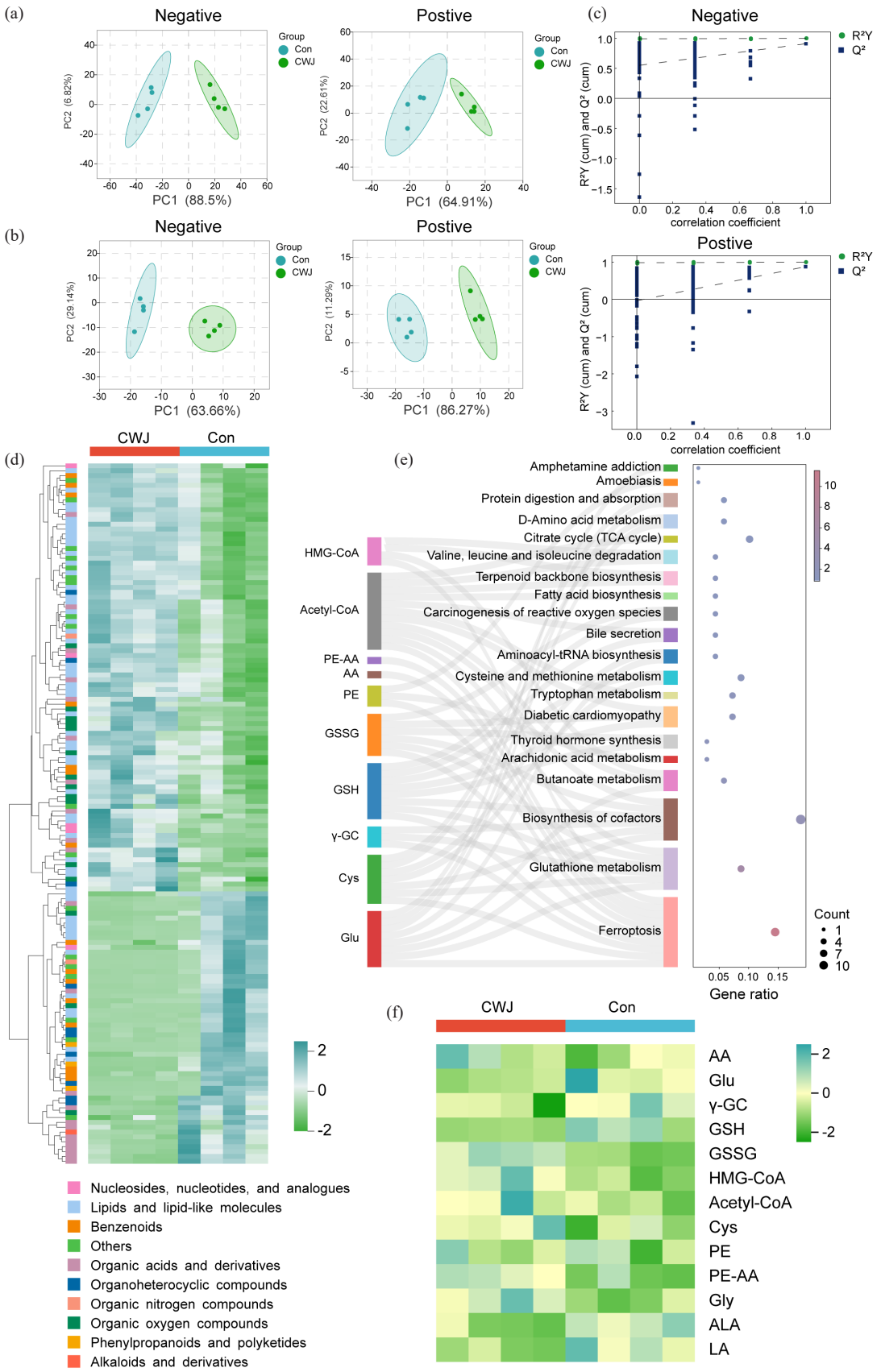

Figure 4. Effects of *E. senticosus* on metabolites of AGS cells. (a) PCA score of metabolites of AGS cells. (b) Partial least squares discriminant analysis (PLS-DA) score of AGS cell metabolites. (c) PLS-DA model validation of metabolites in positive and negative ion modes. (d) Classification and content of differential metabolites. (e) Kyoto encyclopedia of genes and genomes (KEGG) pathway analysis of differential metabolites. (f) Changes in ferroptosis-related metabolites (PC1: Principal Component 1, Con: Control Group, CWJ: *E. senticosus* treated group, HMG-CoA: 3-hydroxy-3-methyl glutaryl coenzyme A, AcetyI-CoA: Acetyl coenzyme A, PE-AA: 1-stearoyl-2-arachidonoyl-sn-glycero-3-phosphoethanolamine, AA: Arachidonic acid, PE: 1-Octadecanoyl-sn-glycero-3-phosphoethanolamine, GSSG: Oxidized glutathione, GSH: Glutathione, γ-GC: γ-glutamylcysteine, Cys: Cysteine, Glu: Glutamate, Gly: Glycine, ALA: α-Linolenic acid, LA: Linoleic acid).

Figure 5. The effect of *E. senticosus* on gene transcription in AGS cells. (a) Differential expression of all genes. (b) Volcano plot of differentially expressed genes. (c) Kyoto encyclopedia of genes and genomes (KEGG) enrichment analysis of differentially expressed genes. (d) Expression changes of ferroptosis-related genes (Con: Control Group, CWJ: *E. senticosus* treated group). EGFR: Epidermal growth factor receptor, TFRC: Transferrin receptor, ACSL4: Long-chain acyl-coa synthetase 4, GPX4: Glutathione peroxidase 4, FTH1: Ferritin heavy chain 1, MAPK1: Mitogen-activated protein kinase 1, HF1A: Hypoxia inducible factor 1 subunit alpha, SLC40A1: Solute carrier family 40 member 1.

and *FTH1* genes exhibited high correlations with all ferroptosis-related metabolites, with R values exceeding 0.6. Specifically, *EGFR* showed correlations with Gly, ALA, and LA, with R values of 0.694169, 0.684101, and 0.652084, respectively. Moreover, the expression of *GPX4* and the content of GSSG were significantly decreased after *E. senticosus* treatment, with an R-value of 0.831427.

We further analyzed the protein expression of ferroptosis-related targets to validate these findings using the Western Blot. The results demonstrated a 63.41% and 87.26% downregulation of *GPX4* and *FTH1*, respectively, whereas *EGFR, TFRC*, and *ACSL4* were upregulated by 84.59%, 72.46%, and 43.57%, respectively (Figure 6b,c).

Furthermore, qRT-PCR results showed that the transcription levels of *GPX4* and *FTH1* were downregulated by 78.29% and 83.41%, respectively, while *EGFR*, *TFRC*, and *ACSL4* were upregulated by 37.59%, 46.23%, and 55.46%, respectively. Although *MAPK1*, *HIF-1A*, and *SLC40A1* gene expressions showed some changes, they did not reach the level of a significant change (Figure 6d). This evidence collectively shows that *E. senticosus* disrupts the balance of these five

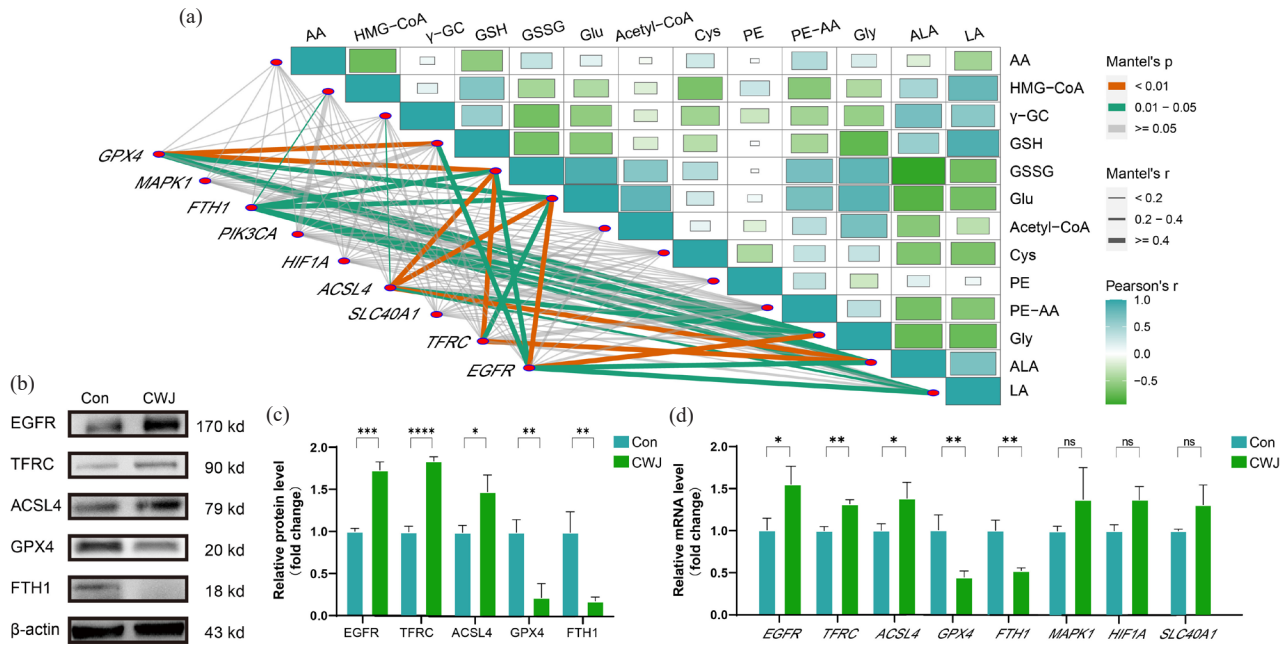

Figure 6. Screening and validation of targets for *E. senticosus*-induced ferroptosis in AGS cells. (a) Correlation analysis of ferroptosis-related gene expression and metabolites. (b) Expression of ferroptosis-related proteins. (c) Optical density values of ferroptosis-related protein expression. (d) mRNA transcript levels of ferroptosis-related genes (*$P < 0.05$, **$P < 0.01$, and ***$P < 0.001$) (Con: Control Group, CWJ: *E. senticosus* treated group, EGFR: Epidermal growth factor receptor, TFRC: Transferrin receptor, ACSL4: Long-chain acyl-coa synthetase 4, GPX4: Glutathione peroxidase 4, FTH1: Ferritin heavy chain 1, MAPK1: Mitogen-activated protein kinase 1, HF1A: Hypoxia inducible factor 1 subunit alpha, SLC40A1: Solute carrier family 40 member 1).

genes within the ferroptosis pathway, thereby triggering ferroptosis in AGS cells.

3.7. Screening of compounds acting on core targets

The results of molecular docking revealed specific interactions (Figure 7a, Figure S7–S11): ARG-200 of EGFR formed hydrogen bonds with syringin, achieving binding with a binding energy of −7.8 kcal/mol. LYS-261 of TFRC formed hydrogen bonds with ciwujianoside I with a binding energy of −10.0 kcal/mol. ACSL4 interacted via hydrogen bonds with ursolic acid involving ASP-362 and GLU-206, resulting in a binding energy of −8.7 kcal/mol. GPX4 formed hydrogen bonds via ASN-113 with ciwujianoside B with a binding energy of −8.3 kcal/mol. FTH1 interacted with quercetin via hydrogen bonds involving SER-113, with a binding energy of −6.2 kcal/mol (Figure 7a). Other compounds showed binding energies greater than −5 kcal/mol, indicating either no binding or less favorable interactions (Figure 7b).

Molecular dynamics simulations further confirmed the stability of these interactions. The RMSD (root mean square deviation) values for EGFR-syringin, TFRC-ciwujianoside I, ACSL4-ursolic acid, GPX4-ciwujianoside B, and FTH1-quercetin complexes were 0.65, 0.43, 0.34, 0.41, and 0.31, respectively (Figure 7c), suggesting highly reliable and strong binding abilities. RMSF (root mean square fluctuation) analysis indicated stable binding states, with all complexes exhibiting RMSF values below 1 nm (Figure 7d). Additionally, simulation analysis in aqueous environments (Figure 7e and f) demonstrated sustained stable interactions over time between these active components of *E. senticosus* and their respective core targets. It is also this effect that makes *E. senticosus* induce GC cells to undergo ferroptosis (Figure 8).

3.8. Comparison with existing research

Since its discovery in 2012 [4], ferroptosis has emerged as a promising novel antitumor strategy due to its ability to selectively target cancer stem cells, potentially enhancing immunotherapy efficacy and overcoming drug resistance [5]. Network pharmacology analysis revealed that various active compounds in *E. senticosus* correspond to different ferroptosis-related targets, suggesting *E. senticosus* its potential to induce ferroptosis in GC cells through multiple pathways and levels. The main active compounds identified include quercetin, syringin, ursolic acid, ciwujianoside B, and ciwujianoside I. Quercetin, a flavonoid, exhibits diverse anti-cancer activities, such as antiproliferative and anti-angiogenic properties, and induces autophagy and apoptosis across various cancers [19]. Syringin, a lignan compound, inhibits the proliferation and migration of MDA-MB-3 and MCF-2 cells and promotes apoptosis of tumor cells [20]. The remaining three are different types of triterpenoid saponins, the most promising candidates for multi-targeted cancer therapy [21]. Ursolic acid has shown broad-spectrum anti-cancer activities targeting various cancer markers [22]. Ciwujianoside B and I are oleanane-type triterpenoid saponins which can affect several intracellular signaling pathways with preventive and antitumor effects *in vitro* and *in vivo* [21].

GO enrichment and KEGG pathway analysis indicated that these compounds may affect the original redox balance in GC cells through mechanisms like iron ion binding and response to oxidative stress, thereby inducing oxidative stress. Affected cells perceive oxidative stress and activate various signaling pathways to respond or restore homeostasis, which is crucial for tumorigenesis, cancer prevention, and treatment [23]. Additionally, ferroptosis is characterized by excessive intracellular peroxide accumulation. Unrestricted lipid peroxidation may eventually damage the cell membrane, causing its rupture and eventually leading to cell death [24]. Bioinformatics analysis showed significantly higher expression of TFRC, GPX4, and ACSL4 in GC tissues compared to normal tissues, suggesting that these genes play a unique role in the pathogenesis and progression of GC.

Cell viability *E. senticosus* assays confirmed that *E. senticosus* had toxic effects on AGS cells, with a dose-dependent increase in the inhibition rate. This study also observed that *E. senticosus* could significantly reduce GSH levels and increase MDA levels, indicating increased lipid peroxidation. The metabolomic analysis further showed that *E. senticosus* treatment significantly increased the synthesis of unsaturated fatty acids precursors (AA, AA-CoA, lystoPE, and PE-AA) following *E. senticosus* treatment, facilitating subsequent lipid peroxide synthesis and cell membrane damage, triggering ferroptosis. Metabolic pathways of unsaturated fatty acids, such as linoleic acid synthesis and arachidonic acid metabolism, involved in lipid peroxidation were significantly enriched among differential metabolic pathways.

GSH, an essential antioxidant essential for peroxide degradation and maintaining an average level of cellular oxidation, plays a vital role in antagonizing ferroptosis [12]. GSH levels and synthetic precursors

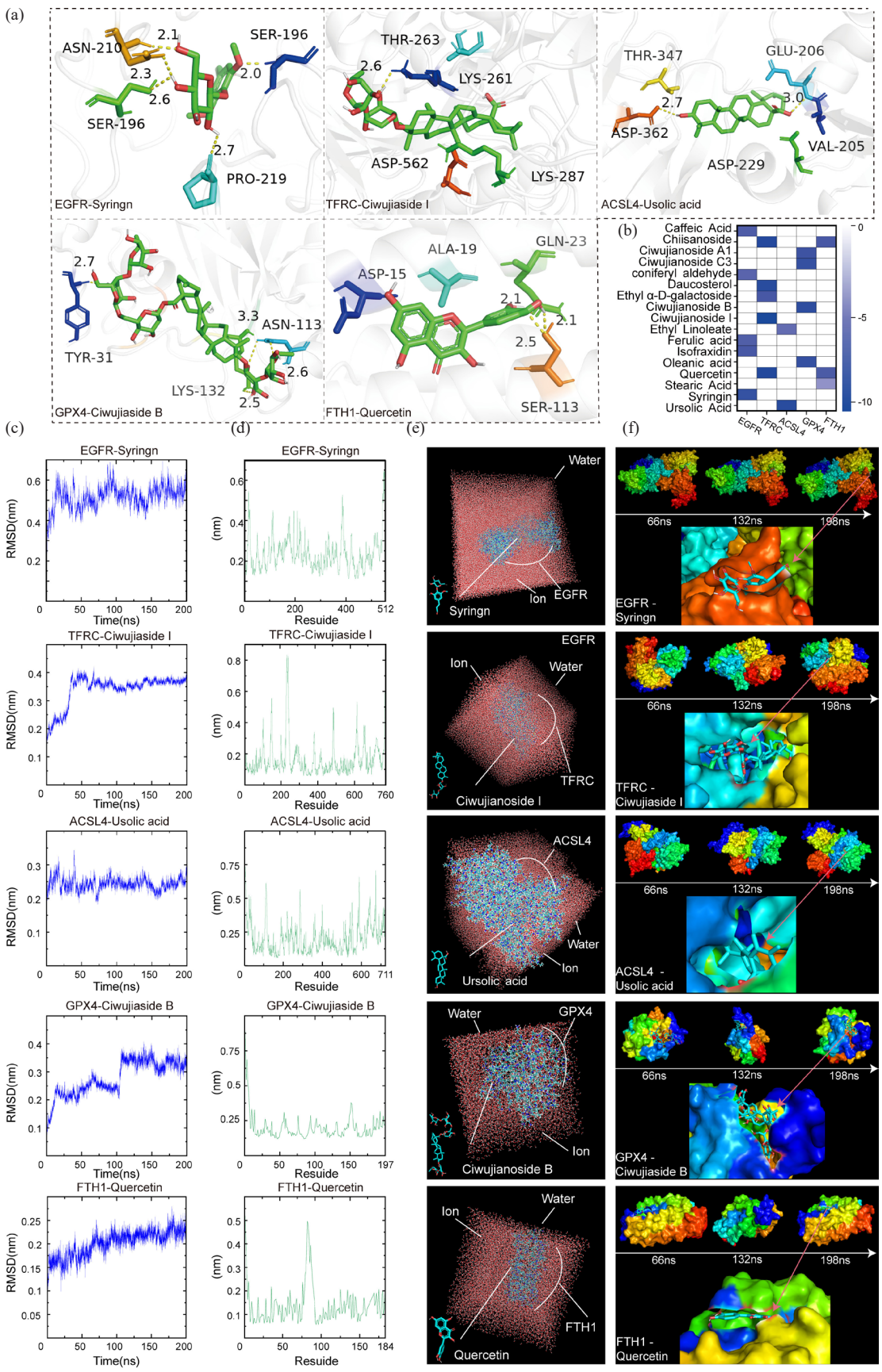

Figure 7. Molecular docking and dynamics analysis of the core active components and targets of *E. senticosus*. (a) Molecular docking of the core active components and corresponding targets. (b) The binding energy of the complex. (c) RMSD analysis of the complex. (d) RMSF analysis of the complex. (e) Combined analysis in a water environment. (f) Effect of time variation on binding. (EGFR: Epidermal growth factor receptor, TFRC: Transferrin receptor, ACSL4: Long-chain acyl-coa synthetase 4, GPX4: Glutathione peroxidase 4, FTH1: Ferritin heavy chain 1, THR: Threonine, SER: Serine, ALA: Alanine, GLN: Glutamine, ASP: Aspartate, ASN: Asparagine, LYS: Lysine, TYR: Tyrosine, GLU: Glutamate, VAL: Valine).

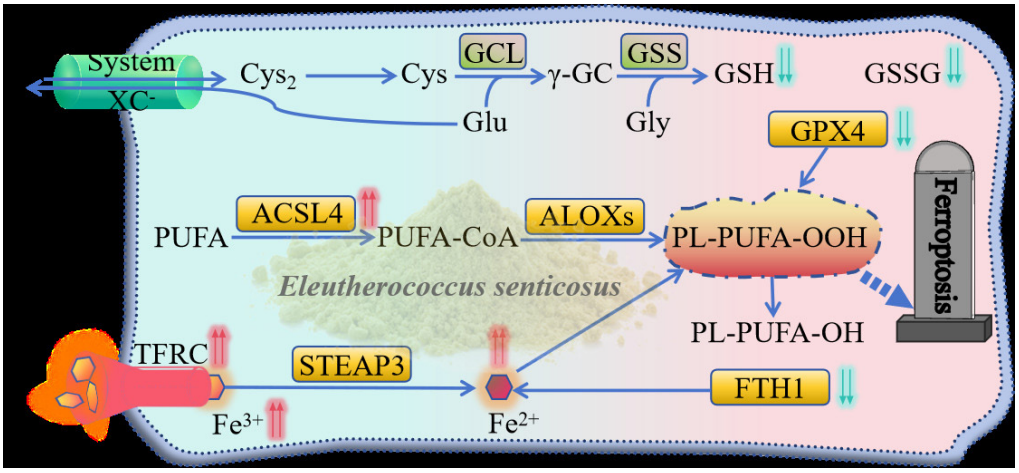

Figure 8. Mechanism of *E. senticosus*-induced ferroptosis in gastric cancer cells. (GPX4: Glutathione peroxidase 4, GSSG: Glutathione, Oxidized, ACSL4: Long-chain acyl-coa synthetase 4, ALOXs: Arachidonate lipoxygenases , GCL: Glutamate-Cysteine Ligase Catalytic Subunit, GSS: Glutathione Synthetase, STEAP3: STEAP3 metalloreductase, TFRC: Transferrin receptor, FTH1: Ferritin heavy chain 1, Cys: Cysteine, Glu: Glutamate, Gly: Glycine, GSH: Glutathione, PL-PUFA-OOH: 1-Octadecanoyl-2-(15S-hydroperoxy-5Z,8Z,11Z,13E-eicosatetraenoyl)-sn-glycero-3-phosphoethanolamine, PL-PUFA-OH: 1-Octadecanoyl-2-(15S-hydroxy-5Z,8Z,11Z,13E-eicosatetraenoyl)-sn-glycero-3-phosphoethanolamine).

(Cys, γ-GC, Glu, and Gly) decreased significantly, ultimately weakening the antioxidant function of GC cells and reducing the difficulty of the onset of ferroptosis. Differential metabolite enrichment in pathways like glutathione metabolism, Cys metabolism, and amino acid synthesis are classical signaling pathways for ferroptosis [8]. Hypoxia, identified as a key driver of ferroptosis susceptibility (Shi, 2024), was enriched by differential metabolites in the HIF pathway following *E. senticosus* treatment, highlighting its regulatory role in ferroptosis. These findings indicate that *E. senticosus* treatment significantly impacts the metabolic pathways related to ferroptosis in AGS cells.

Similar to the changes in metabolites, ferroptosis-related genes also exhibited significant changes in AGS cells treated with *E. senticosus*, consistent with the findings of network pharmacology and bioinformatics predictions. Correlation analysis identified *EGFR*, *TFRC*, *ACSL4*, *GPX4*, and *FTH1* as the most significant ferroptosis-related genes in GC cells following *E. senticosus* treatment, consistent with their prediction as core target genes in network pharmacology. Western Blotting and qRT-PCR results demonstrated a significant increase in protein and gene expression levels of *EGFR*, *TFRC*, and *ACSL4* in AGS cells post *E. senticosus* treatment. Conversely, the protein and gene expression of ferroptosis antagonistic genes *GPX4* and *FTH1* significantly decreased, consistent with the findings from transcriptome sequencing in this study and previous research [14]. *GPX4* functions as a crucial enzyme in lipid peroxides. In the presence of GSH, it is converted into oxidized glutathione GSSG and reduced lipid peroxides to lipid alcohols to prevent ferroptosis [25]. *E. senticosus* joint analysis revealed a significant decrease in *GPX4* expression and GSSG content; the two were significantly correlated. Inhibiting *GPX4* to induce ferroptosis has emerged as a novel therapeutic strategy for tumor cell death [17]. *E. senticosus* treatment led to a significant increase in *TFRC* expression. In contrast, overexpression of *TFRC* promotes the translocation of iron ions into the cell, triggering a significant increase in ROS species production—such as hydroxyl and hydroperoxyl radicals—via the Fenton reaction, which initiates a cascading peroxidation chain reaction [24]. Meanwhile, the decrease in *FTH1* expression is attributed to ferritin autophagy, a lysosomal pathway that degrades ferritin and releases ferric ions, thereby inducing iron overload [7]. *E. senticosus* could affect the expression of the *FTH1* gene through this mechanism. Lipid peroxidation of long-chain phospholipids, involving *ACSL4* and lipoxygenase activation, plays an important role in ferroptosis [26]. The high expression of *ACSL4* can promote cell ferroptosis, while in AGS cells treated with *E. senticosus*, the expression of *ACSL4* significantly increased, suggesting that it promoted the occurrence and development of ferroptosis. Therefore, *EGFR*, *TFRC*, *ACSL4*, *GPX4*, and *FTH1* are the core targets of GC cell ferroptosis induced by *E. senticosus*.

The results of molecular docking showed that all the active components of *E. senticosus* were able to bind into the docking pocket, with binding energies all less than −5 kcal/mol, indicating plausible binding interactions [27]. Syringin binds at the junction of two subunits of *EGFR* and affects its function. *TFRC* exhibited the lowest binding energy with ciwujianoside I, suggesting that the two require minimal energy to bind tightly. Ciwujianoside I was firmly encapsulated into the *TFRC* protein, speculating that this interaction significantly improves the iron ion transport capacity of *TFRC*, thereby promoting ferroptosis. Ursolic acid was identified as the compound binding to *ACSL4*, potentially enhancing the synthesis of unsaturated fatty acids upon interaction. The docking binding energy of *FTH1* and quercetin was −6.2 kcal/mol, indicating an effective combination. In AGS cells, quercetin is likely to induce iron release by promoting ferritin autophagy, ultimately promoting ferroptosis. Ciwujianoside B binds to *GPX4*. Timosaponin, a compound of the same type, can target the degradation of *GPX4* by forming a complex with *HSP90*, ultimately inducing ferroptosis in non-small cell lung cancer [6]. It is speculated that ciwujianoside B inhibits the oxidative function of *GPX4* by binding to it, thus promoting ferroptosis in GC cells.

The RMSD results showed that the binding between the five compounds and the five core targets reached a stable level, indicating consistent stability of the compounds in the active sites of the corresponding targets [27]. Meanwhile, the low RMSF value of the complexes indicates that the interactions are stable and long-lasting [16]. Therefore, it is inferred that syringin, ciwujianoside I, ursolic acid, quercetin, and ciwujianoside B are the pivotal compounds of *E. senticosus* inducing ferroptosis in GC cells treated with *E. senticosus*.

4. Conclusions

In summary, *E. senticosus* appears to upregulate TFRC expression via ciwujianoside I, facilitating increased cellular iron ion transport. Quercetin reduces *FTH1* expression, releasing ferrous ions and interfering with iron metabolism. Ursolic acid promotes *ACSL4* expression, promoting unsaturated fatty acid synthesis and increasing cellular peroxides for ferroptosis. Combining *GPX4* with ciwujianoside B reduces oxidation ability, causing excessive incorporation of phospholipid hydroperoxides into cell membranes, ultimately triggering ferroptosis in AGS cells. However, the mechanism of action of *EGFR* involved in the ferroptosis process is unclear Notably, the toxic effects of *E. senticosus* were observed only *in vitro* in AGS cells. Future studies should explore various animal models and isolate individual components for further validation.

CRediT authorship contribution statement

Xin Song: Writing—original draft, software, methodology, data curation, conceptualization, investigation. **Yufeng Li:** Software, methodology, data curation, conceptualization, investigation. **Dan Li:** Software, methodology, investigation. **Zhuo Wang:** Software, methodology, investigation. **Xuekun Kou:** Software, methodology, investigation. **Xiaohui Zhang:** Software, methodology. **Yuanyuan Zhao:** Software, methodology. **Chunqiu Liu:** Software, methodology. **Yuehong Long:** Writing—review and editing, data curation, supervision, conceptualization. **Jingwu Li:** Writing—review and editing, data curation, supervision, conceptualization. **Zhaobin Xing:** Writing—review and editing, data curation, supervision, conceptualization, original draft, funding acquisition.

Declaration of competing interest

The authors declare that they have no known competing financial interests or personal relationships that could have appeared to influence the work reported in this paper. All data were generated in-house and no paper mill was used. All authors agree to be accountable for all aspects of work ensuring integrity and accuracy.

Data availability

The sequence data from RNA-Seq experiments reported in this study have been deposited in the NCBI with accession no. PRJNA1129195. The original data of the compounds reported in this study have been preserved in the EMBL-EBI metabolic database, and the preservation number is MTBLS10552.

Declaration of Generative AI and AI-assisted technologies in the writing process

The authors confirm that there was no use of AI-assisted technology for assisting in the writing of the manuscript and no images were manipulated using AI.

Acknowledgement

This work was supported by Hebei Natural Science Foundation H2024105019, Hebei Province intelligence introduction project 22170201C and Tangshan Key R&D Program 22150211A.

Appendix A. Supplementary material

Supplementary material to this article can be found online at https://dx.doi.org/10.25259/AJC_9_2024

References

1. Ferlay, J., Colombet, M., Soerjomataram, I., Parkin, D.M., Piñeros, M., Znaor, A., Bray, F., 2021. Cancer statistics for the year 2020: An overview. *International Journal of Cancer,* **149** (4), 778–789. https://doi.org/10.1002/ijc.33588.
2. Zeng, Y., Jin, R.U., 2022. Molecular pathogenesis, targeted therapies, and future perspectives for gastric cancer. *Seminars in Cancer Biology,* **86** (Pt3), 566–582. https://doi.org/10.1016/j.semcancer.2021.12.004.
3. Yu, P., Hu, C., Ding, G., Shi, X., Xu, J., Cao, Y., Chen, X., Wu, W., Xu, Q., Fang, J., Huang, X., Yuan, S., Chen, H., Wang, Z., Huang, L., Pang, F., Du, Y., Cheng, X., 2024. Mutation characteristics and molecular evolution of ovarian metastasis from gastric cancer and potential biomarkers for paclitaxel treatment. *Nature Communication,* **15** (1), 3771. https://doi.org/10.1038/s41467-024-48144-0.
4. Liang, D., Feng, Y., Zandkarimi, F., Wang, H., Zhang, Z., Kim, J., Cai, Y., Gu, W., Stockwell, B.R., Jiang, X., 2023. Ferroptosis surveillance independent of GPX4 and differentially regulated by sex hormones. *Cell,* **186** (13), 2748–2764. https://doi.org/10.1016/j.cell.2023.05.003.
5. Wang, W., Green, M., Choi, J.E., Gijón, M., Kennedy, P.D., Johnson, J.K., Liao, P., Lang, X., Kryczek, I., Sell, A., Xia, H., Zhou, J., Li, G., Li, J., Li, W., Wei, S., Vatan, L., Zhang, H., Szeliga, W., Gu, W., Liu, R., Lawrence, T.S., Lamb, C., Tanno, Y., Cieslik, M., Stone, E., Georgiou, G., Chan, T.A., Chinnaiyan, A., Zou, W., 2019. $CD8^+$ T cells regulate tumour ferroptosis during cancer immunotherapy. *Nature,* **569** (7755), 270–274. https://doi.org/10.1038/s41586-019-1170-y.
6. Zhou, C., Yu, T., Zhu, R., Lu, J., Ouyang, X., Zhang, Z., Chen, Q., Li, J., Cui, J., Jiang, F., Jin, K.Y., Sarapultsev, A., Li, F., Zhang, G., Luo, S., Hu, D., 2023. Timosaponin AIII promotes non-small-cell lung cancer ferroptosis through targeting and facilitating HSP90 mediated GPX4 ubiquitination and degradation. *International Journal of Biological Sciences* **19** (5), 1471–1489. https://doi.org/10.7150/ijbs.77979.
7. Nakamura T., Conrad, M., 2024. Exploiting ferroptosis vulnerabilities in cancer. *Nature Cell Biology* **26** (9), 1401–1419. https://doi.org/10.1038/s41556-024-01425-8.
8. Chen, C., Liu, J., Lin, X., Xiang, A., Ye, Q., Guo, J., Rui, T., Xu, J., Hu, S., 2024. Crosstalk between cancer-associated fibroblasts and regulated cell death in tumors: Insights into apoptosis, autophagy, ferroptosis, and pyroptosis. *Cell Death Discovery* **10** (1), 189. https://doi.org/10.1038/s41420-024-01958-9.
9. Gao, W., Wang, X., Zhou, Y., Wang, X., Yu, Y., 2022. Autophagy, ferroptosis, pyroptosis, and necroptosis in tumor immunotherapy. *Signal Transduction and Targeted Therapy* **7** (1), 196. https://doi.org/10.1038/s41392-022-01046-3.
10. Zhu, Y., Yue, P., Dickinson, C.F., Yang, J.K., Datanagan, K., Zhai, N., Zhang, Y., Miklossy, G., Lopez-Tapia, F., Tius, M.A., Turkson, J., 2022. Natural product preferentially targets redox and metabolic adaptations and aberrantly active STAT3 to inhibit breast tumor growth in vivo. *Cell Death and Disease* **13** (12), 1022. https://doi.org/10.1038/s41419-022-05477-2.
11. Meng, Q., Pan, J., Liu, Y., Chen, L., Ren, Y., 2018. Anti-tumour effects of polysaccharide extracted from Acanthopanax senticosus and cell-mediated immunity. *Experimental and Therapeutic Medicine* **15** (2), 1694–1701. https://doi.org/10.3892/etm.2017.5568.
12. Guo, H.Y., Zhang, J., Lin, L.M., Song, X., Zhang, D.D., Cui, M.H., Long, C.W., Long, Y.H., Xing, Z.B., 2022. Metabolome and transcriptome analysis of eleutheroside B biosynthesis pathway in Eleutherococcus senticosus. *Heliyon*, **8** (6), e09665. https://doi.org/10.1016/j.heliyon.2022.e09665.
13. Lee, C.H., Huang, C.W., Chang, P.C., Shiau, J.P., Lin, I.P., Lin, M.Y., Lai, C.C., Chen, C.Y., 2019. Reactive oxygen species mediate the chemopreventive effects of syringin in breast cancer cells. *Phytomedicine*, **61**, 152844. https://doi.org/10.1016/j.phymed.2019.152844.
14. Su, J., Zhang, X., Kan, Q., Chu, X., 2022. Antioxidant activity of Acanthopanax senticosus flavonoids in H_2O_2-induced RAW 264.7 Cells and DSS-induced colitis in mice. *Molecules* **27** (9), 2872. https://doi.org/10.3390/molecules27092872.
15. Barathikannan, K., Chelliah, R., Vinothkanna, A., Prathiviraj, R., Tyagi, A., Vijayalakshmi, S., Lim, M.-J., Jia, A.-Q., Oh, D.-H., 2024. Untargeted metabolomics-based network pharmacology reveals fermented brown rice towards anti-obesity efficacy. *NPJ Science of Food* **8** (1), 20. https://doi.org/10.1038/s41538-024-00258-x.
16. Zare, F., Ataollahi, E., Mardaneh, P., Sakhteman, A., Keshavarz, V., Solhjoo, A., Emami, L., 2024. A combination of virtual screening, molecular dynamics simulation, MM/PBSA, ADMET, and DFT calculations to identify a potential DPP4 inhibitor. *Scientific Reports,* **14** (1), 7749. https://doi.org/10.1038/s41598-024-58485-x.
17. Wang, S., Zhao, X., Li, C., Dong, J., Ma, J., Long, Y., Xing, Z., 2024. DNA methylation regulates the secondary metabolism of saponins to improve the adaptability of Eleutherococcus senticosus during drought stress. *BMC Genomics*, **25** (1), 330. https://doi.org/10.1186/s12864-024-10237-x.
18. Zhang, J., Jiao, M., Cheng, W., Song, X., Wang, S., Zhao, X., Dong, J., Zhang, X., Long, Y., Xing, Z., 2023. Identification and functional analysis of glycosyltransferase catalyzing the synthesis of phlorizin and trilobatin in Lithocarpus polystachyus Rehd. *Industrial Crops and Products,* **192**, 116056. https://doi.org/10.1016/j.indcrop.2022.116056.
19. Rauf, A., Imran, M., Khan, I. A., Ur-Rehman, M., Gilani, S.A., Mehmood, Z., Mubarak, M.S., 2018. Anticancer potential of quercetin: A comprehensive review. *Phytother Research* **32** (11), 2109–2130. https://doi.org/10.1002/ptr.6155.
20. Wang, F., Yuan, C., Liu, B., Yang, Y.F., Wu, H.Z., 2022. Syringin exerts anti-breast cancer effects through PI3K-AKT and EGFR-RAS-RAF pathways. *Journal of Translational Medicine,* **20** (1), 310. https://doi.org/10.1186/s12967-022-03504-6.
21. Khwaza, V., Oyedeji, O.O., Aderibigbe, B.A., 2020. Ursolic acid-based derivatives as potential anti-cancer agents: An update. *International Journal of Molecular Sciences* **21** (16), 5920. https://doi.org/10.3390/ijms21165920.
22. Alam, M., Ali, S., Ahmed, S., Elasbali, A.M., Adnan, M., Islam, A., Hassan, M.I., Yadav, D.K., 2021. Therapeutic potential of ursolic acid in cancer and diabetic neuropathy diseases. International Journal of Molecular Sciences **22** (22), 12162. https://doi.org/10.3390/ijms222212162.
23. Wang, R., Liang, L., Matsumoto, M., Iwata, K., Umemura, A., He, F., 2023. Reactive oxygen species and NRF2 signaling, friends or foes in cancer? *Biomolecules*, **13** (2), 353. https://doi.org/10.3390/biom13020353.
24. Jiang, X., Stockwell, B.R., Conrad, M., 2021. Ferroptosis: mechanisms, biology and role in disease. *Nature Reviews. Molecular Cell Biology,* **22** (4), 266–282. https://doi.org/10.1038/s41580-020-00324-8.
25. Chen, X., Kang, R., Kroemer, G., Tang, D., 2021. Broadening horizons: The role of ferroptosis in cancer. *Nature Reviews. Clinical Oncology,* **18** (5), 280–296. https://doi.org/10.1038/s41571-020-00462-0.
26. Li, S., Ouyang, X., Sun, H., Jin, J., Chen, Y., Li, L., Wang, Q., He, Y., Wang, J., Chen, T., Zhong, Q., Liang, Y., Pierre, P., Zou, Q., Ye, Y., Su, B., 2024. DEPDC5 protects CD8+ T cells from ferroptosis by limiting mTORC1-mediated purine catabolism. *Cell Discovery,* **10** (1), 53. https://doi.org/10.1038/s41421-024-00682-z.
27. Yan, B., Ai, Y., Sun, Q., Ma, Y., Cao, Y., Wang, J., Zhang, Z., Wang, X., 2021. Membrane damage during ferroptosis is caused by oxidation of phospholipids catalyzed by the oxidoreductases POR and CYB5R1. *Molecular Cell* **81** (2), 355–369. https://doi.org/10.1016/j.molcel.2020.11.024